Dragonfly Mission Entry and Descent Modeling and Simulation Overview

Alejandro R. Pensado*, Richard Winski†, James Williams‡, Caleb Robb‡
Analytical Mechanics Associates, Hampton, VA, 23666

Dragonfly is a New Frontiers Program mission, led by The Johns Hopkins Applied Physics Laboratory, that will deliver a rotorcraft lander to Saturn's moon, Titan. The focus of this work is to analyze the trajectory of the entry vehicle from cruise stage separation until lander separation. This analysis is done by the NASA Langley Research Center Entry, Descent, and Landing team using the Program to Optimize Trajectories II. This paper provides an overview of the current design and the robustness of the overall entry sequence using a Monte Carlo uncertainty analysis. The work presented in this study includes the updated design, models, and analysis completed since the Dragonfly Entry, Descent, and Landing Mission Preliminary Design Review.

I. Introduction

Titan has been a high priority for the planetary science community as the only moon in the solar system with a dense atmosphere that has standing bodies of liquid on the surface [1]. As such, there is strong interest to study Titan. Dragonfly was selected as the fourth New Frontiers Program mission, led by The Johns Hopkins Applied Physics Laboratory (APL), to deliver a rotorcraft to Titan. Due to the unique environment of Titan, there are unique challenges related to safely delivering the rotorcraft to the moon's surface. The focus of this work is to model and analyze the trajectory the Dragonfly entry vehicle from prior to cruise stage separation to lander separation. Dragonfly has two launch opportunities: a primary launch window in 2028 and a backup opportunity in 2029 targeted to reaching Titan in the mid 2030s. Dragonfly is expected to arrive roughly one Titan year after the Huygens probe's entry, and will encounter similar seasonal and atmospheric conditions as Huygens[2]. The Dragonfly entry vehicle consists of the aeroshell and the lander. The aeroshell is a 4.5 m diameter, 60 degree sphere-cone based on the Genesis Sample Return Capsule (GSRC), which was modified to meet Dragonfly requirements for the lander geometry and mission performance [3]. At this point of the design process, there are two entry vehicle mass properties used in the design analysis, the current best estimate (CBE) 2309 kg and Maximum Possible Value (MPV) of 2600 kg. These values are expected to converge as the design refines as the mission approaches Critical Design Review (CDR). This paper provides an overview of the design, the current modeling, and the performance of the entry sequence since the Preliminary Design Review (PDR) in 2023 [4].

II. Dragonfly Concept of Operations

The Entry, Descent, and Landing (EDL) segment, shown in Fig 1, begins in the entry preparation phase where the spacecraft (cruise stage, aeroshell, and lander) wakes up from hibernation and performs a maneuver to precess to entry attitude and spin up from the cruise phase of 1.5 Revolutions Per Minute (RPM) to 2 RPM for additional entry stability. The entry vehicle is separated from the cruise stage using a spring mechanism approximately 10 minutes prior to entry and is designed to eliminate far-field recontact risk by selecting the separation time and the sizing of the separation springs. After entry interface at 1270 km, the vehicle nominally undergoes approximately 10 Earth G's of deceleration and peak heat flux of 280 W/cm^2.

The 8.25m Disk-Gap-Band (DGB) drogue parachute deploys around the target of Mach 1.5 with a five second window to minimize the total angle of attack and back up timer at the end of the window. The vehicle descends under drogue parachute for approximately 108 minutes. The drogue parachute is released and pulls out the main parachute at a predetermined pressure which is measured on board with a pressure transducer. Due to Titan's cold environment, there are power and thermal constraints that limit the duration of the descent. Therefore, the parachutes are sized for

*Aerospace Engineer, Atmospheric Flight and Entry Systems Branch, MS 489, Senior AIAA Member.
†Aerospace Engineer, Atmospheric Flight and Entry Systems Branch, MS 489, AIAA Associate Fellow.
‡Aerospace Engineer, Atmospheric Flight and Entry Systems Branch, MS 489, AIAA Member.

system stability and to ensure a descent rate while meeting the overall time constraint. Furthermore, the main parachute deployment needs to occur at a high enough altitude such that the heatshield separation occurs subsequently with enough margin for the remaining required operations. The heatshield is deployed 120 s after the main parachute deployment and this separation event starts the phase called Preparation for Powered Flight (PPF).

During PPF, the lander is lowered into a posed configuration such the lander rotors will be in the airflow and can be turned on without any contact risk. The lander uses the rotors to null out the spin rate of the entry vehicle to support the successful operation of the optical navigation system to meet requirements for lander separation. The timings for the PPF events are driven by the capabilities of the sensors, such as the lidar altimeter range, predictions of the time to despin the vehicle, and the time required by the navigation filter to integrate the optical navigation data. The lander release trigger is enabled at a nominal 1000 m altitude and a planet-relative down velocity of 2.9 m/s. The trigger is designed within an altitude window from approximately 1000 m to 800 m with limits on the attitude rates. The trigger logic includes a constraint of two seconds since the last despin event before releasing. If the desired conditions are not met by 800 m, then the lander will prioritize the altitude to allow for successful transition to powered flight (TPF) operations. The TPF phase has a critical need for sufficient altitude to allow the lander to maneuver away from the backshell and main parachute and transition into free flight operations and search for its first landing site.

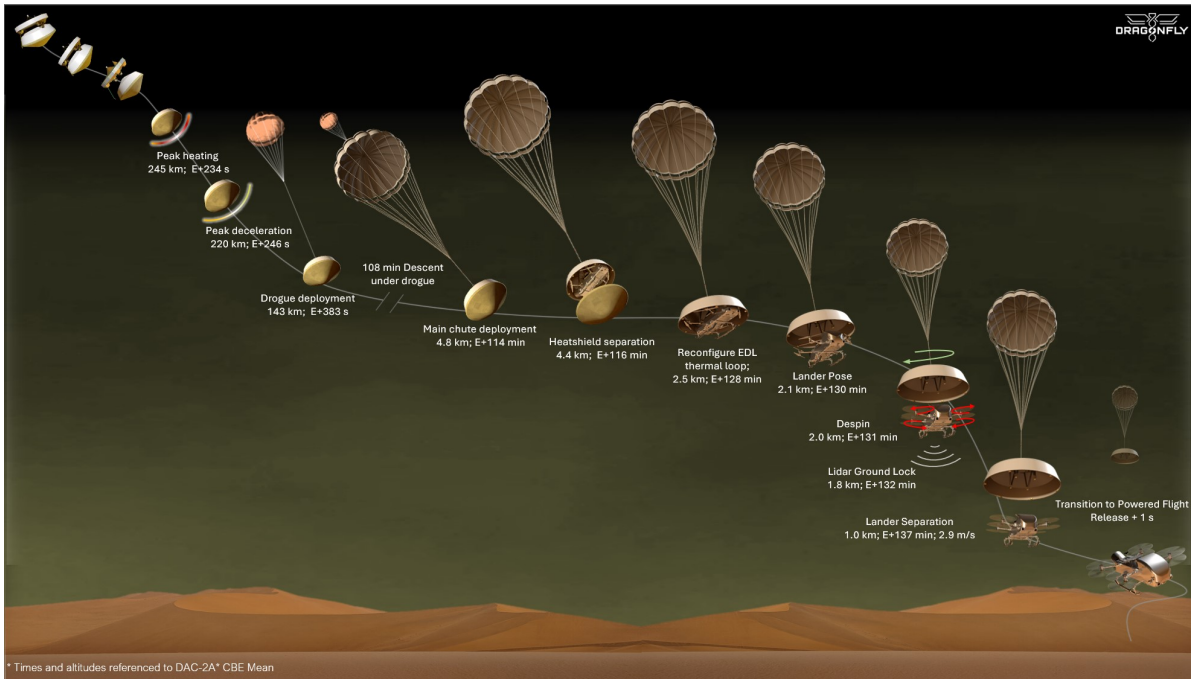

Fig. 1 Dragonfly EDL Concept of Operations

III. EDL Flight Mechanics Modeling

The Program to Optimize Simulated Trajectories II (POST2) is the tool used for the primary EDL simulation for Dragonfly [5]. This program is a six-degree-of-freedom (6DOF) simulation tool used to target and optimize trajectories. It is a generalized point-mass, discrete-parameter targeting and trajectory optimization simulation program with multi-vehicle capabilities that integrates translational and rotational equations of motion along the trajectory. POST2 has a been used as a prime simulation tool for a variety of successful EDL flight missions such as Mars Science Laboratory [6] and more recently Mars 2020 [7]. The simulation framework is modular in that it can incorporate a variety of subsystem models such as vehicle, planet, and atmospheric models and is used during mission planning to assess the system's performance against requirements and response to off-nominal conditions. The EDL POST2 simulation begins approximately 10 s prior to cruise stage separation and continues down to lander release with additional tracking of the drogue parachute, mortar lid, heatshield, and backshell with main parachute down to the ground to support lander contact analyses. Since PDR[4], the EDL design and simulation models have undergone several updates, including an

increased drogue parachute size, updated entry vehicle aerodynamic database, parachute properties, post-heatshield jettison aerodynamics, despin controller, and lander release logic[8]. This paper summarizes the state of the key EDL models.

The POST2 simulation includes the following models:

- Initial States
- Gravity Model
- 3rd Body Gravity Model
- Titan Atmosphere
- Capsule Aerodynamics
- Backshell and Lander Aerodynamics
- Heatshield Aerodynamics
- Aerothermal Indicators
- Parachute Models (Drogue & Main)
- Despin Controller
- Lander Separation Logic

A. Vehicle Modeling

The entry vehicle design, a 4.5 m 60° half-angle sphere cone based on the Genesis Sample Return Capsule, was modified to meet requirements for lander geometry and mission heating. Fig 2 shows the four configurations. The spacecraft consists of the cruise stage with the entry vehicle, both modeled as separate rigid bodies. The entry vehicle consists of the backshell, lander, and heatshield and is modeled as a single rigid body. Once the heatshield jettisons, the stowed vehicle and heatshield are modeled as separate rigid bodies for recontact analysis. Lastly, when the lander is lowered into the posed position the backshell and lander are modeled as a single rigid body. The changes in mass properties at separation events occur instantaneously in the simulation. The vehicle is analyzed using two sets of mass properties, the Maximum Possible Value (MPV) of 2600 kg and the Current Best Estimate (CBE) of 2309 kg.

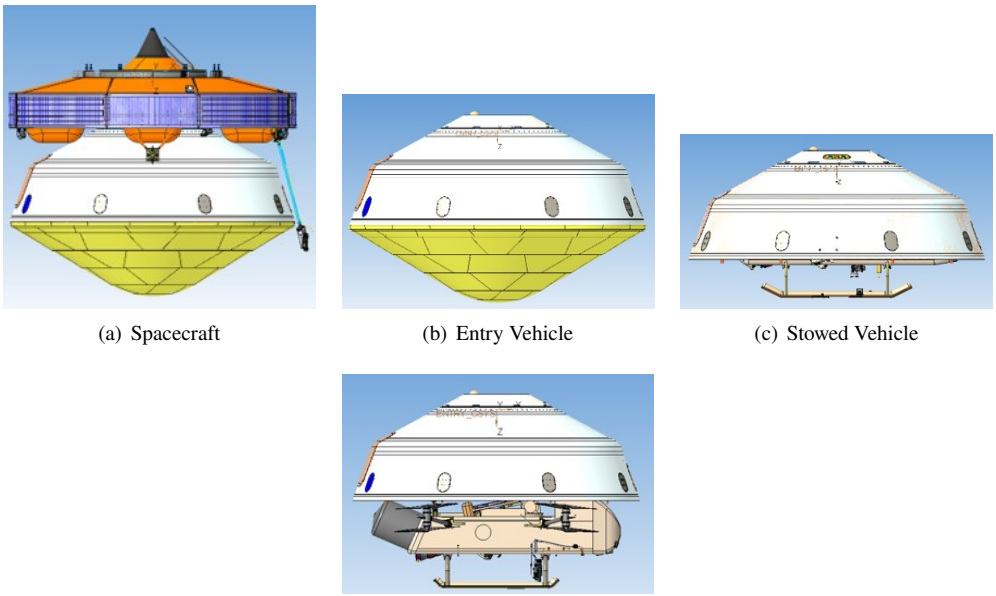

(a) Spacecraft (b) Entry Vehicle (c) Stowed Vehicle

(d) Posed Vehicle

Fig. 2 Vehicle Configurations

B. Initial States

The initial states are defined in collaboration with the Mission Design and Navigation (MDNav) team. The MDNav team uses a combination of Evolutionary Mission Trajectory Generator (EMTG) [9], and Jet Propulsion Laboratory (JPL) Monte [10] to design the interplanetary trajectory with the corresponding trajectory correction maneuvers (TCMs) to reach Titan in the same Titan-relative inertial position for the 2028 Primary launch or 2029 Backup launch opportunities[11]. The handoff point was chosen at a radius 7800 km between the MDNav and EDL simulation. This was chosen as a fixed radius such that the interplanetary trajectories, regardless of launch opportunities, terminate at the

exact same handoff state relative to Titan. The MDNav and EDL teams collaborate to ensure the end-to-end trajectory targets the lander separation site.

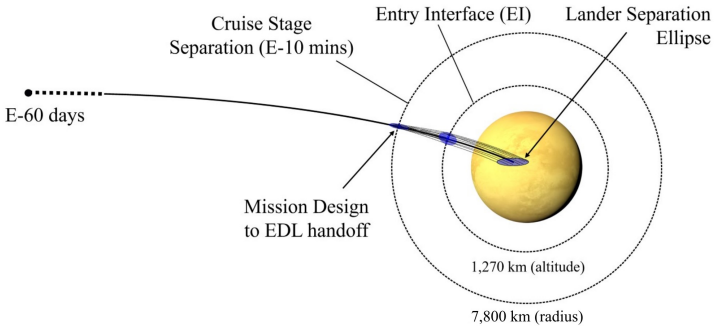

Fig. 3 Entry HandOff

C. Gravity Model

A Titan 4x4 gravitational model is used for the simulation. This is used across the team and has been verified comparing POST2 with JPL Monte results during Titan approach [12]. Fig 4 shows the gravitational accelerations as a function of the longitude and latitude. Similarly, spherical gravitational accelerations for 3rd bodies are used during Titan as part of the end-to-end targeting. Furthermore, the 3rd bodies are used to minimize acceleration differences between simulations to maintain continuity between the hand off point between MDNav and the EDL simulations. The following bodies are modeled in POST2:

- Sun
- Saturn
- Jupiter Barycenter
- Rhea
- Iapetus
- Dione
- Tethys
- Enceladus
- Mimas
- Phoebe
- Hyperion
- Helene

JPL Monte models additional gravitational bodies, but a minimal effect has been noted during short Titan approach and entry phases. The 3rd body perturbations are only modeled up to entry interface where the accelerations are overshadowed by aerodynamic and atmospheric forces.

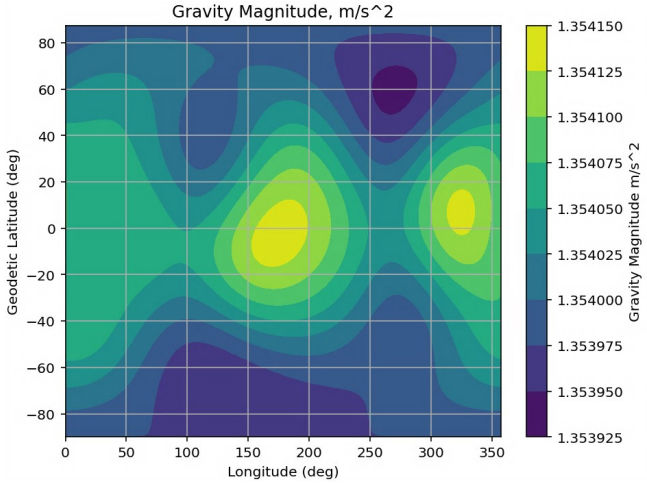

Fig. 4 Titan 4x4 gravitational accelerations

D. Atmosphere Model

As discussed in Ref. [2], Dragonfly is expected to arrive at Titan in the same season Huygens landed. This is intended to be able to leverage data collected during Huygens. An updated atmosphere model has been developed for Dragonfly which incorporates the Huygens model with updates combining data collected and processed since Huygens. The parameters that are modeled include the temperature, density, pressure, speed of sound, chemical composition, wind, and turbulence. Temperature and density, including the minimum, nominal, and maximum profiles, are provided as a function of altitude. Fig 5 shows the statistical temperature and density profile from 10,000 Monte Carlo samples.

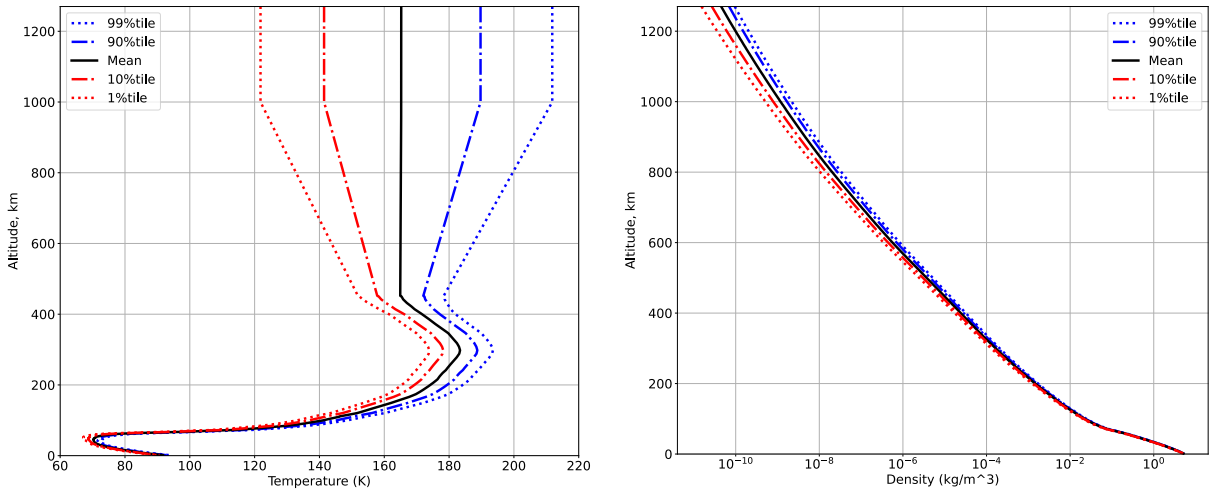

(a) (b)

Fig. 5 Nominal, 1%-tile, and 99%-tile profiles for a) Temperature and b) Density

The pressure and speed of sound, which impact aerodynamics, are calculated as a function of the temperature and density profiles. The pressure is calculated using the Van der Waals equation, summarized in Eqn. 1.

$$P = \frac{T_{nom} R}{\frac{M}{\rho_{disp}} - 3.913 \times 10^{-5}} - 0.1390 \times \left(\frac{\rho_{disp}}{M}\right)^2 \tag{1}$$

Where P is the atmospheric pressure, T_{nom} is the nominal temperature, $R = 8.31472\ J/(mol \cdot K)$ is the universal gas constant, $M = 0.20278\ kg/mol$ is the molecular mass of the titan atmosphere, and ρ_{disp} is the dispersed density. The constants corresponds to the Van der Waals correction for Nitrogen.

The speed of sound is calculated as a function of the dispersed temperature and the atmospheric specific heat ratio as summarized in Eqn. 2.

$$C = \sqrt{\frac{\gamma R T_{disp}}{M}} \tag{2}$$

The winds and gusts are modeled separately, then combined to form the total wind profile. The wind profiles are split into three directions: Zonal, Meridional, and Vertical. The winds are positive East, North, and Down, respectively. Fig. 6 shows statistical representations of the wind profiles as a function of altitude.

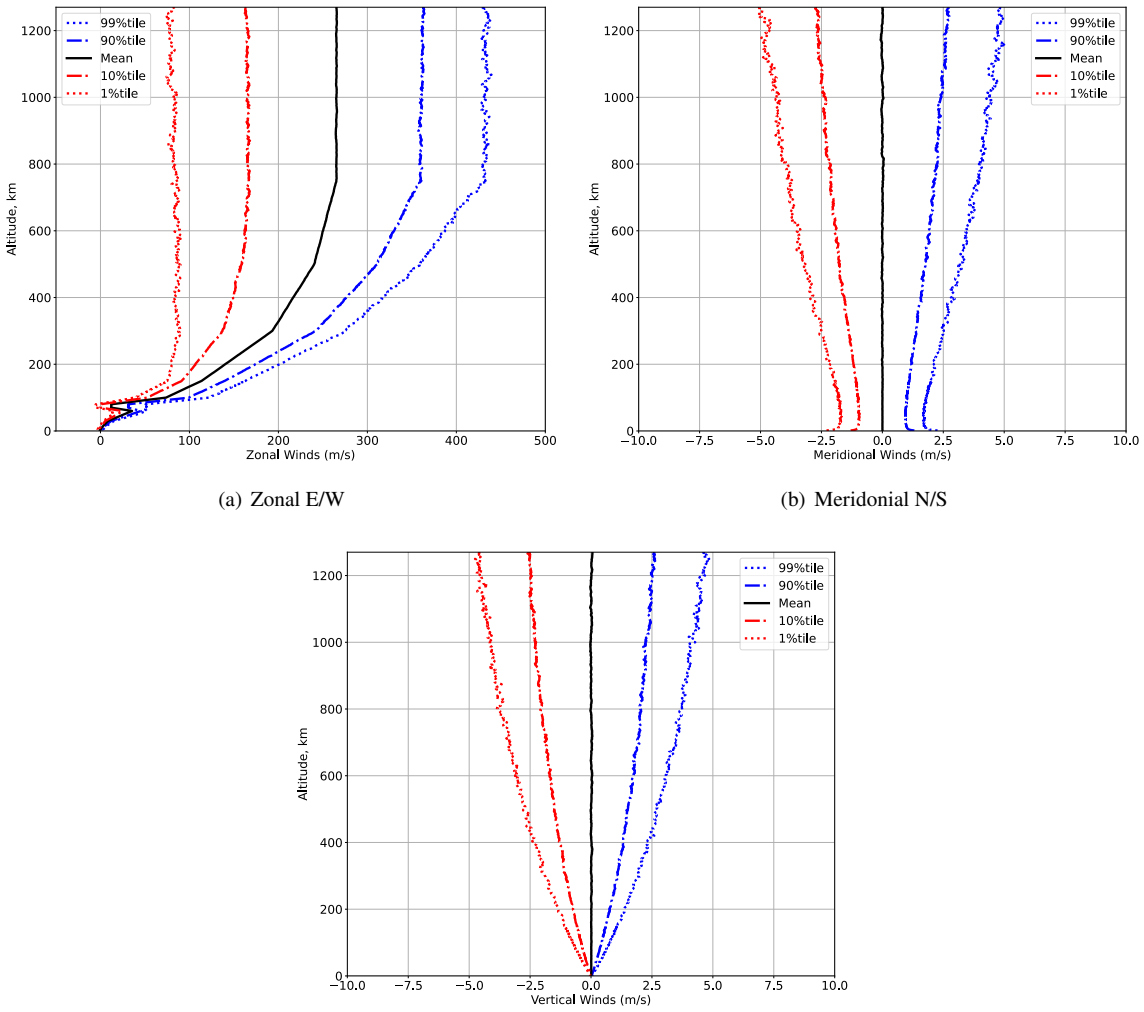

(a) Zonal E/W

(b) Meridonial N/S

(c) Vertical Wind

Fig. 6 Nominal, 1%-tile, 10%-tile, 90%-tile, and 99%-tile wind-plus-gust profiles for a) Zonal, b) Meridional, and c) Vertical directions

E. Aerothermodynamics

The aerothermodynamics team provides indicators for points along the outer mold line (OML) including the stagnation point, fore shoulder, aft shoulder, and aft lid. These indicators are derived from analysis performed using DPLR and NEQAIR[13]. The margined convective and radiative heating are then calculated using curve fit models along with the indicators. POST2 utilizes Chemical Equilibrium Application (CEA) [14] to calculate post-shock parameters such as temperature, density, and mass fractions used in the models. The models are used to calculate the convective and radiative heating for all points. These results are then verified with the aerothermodynamics team and used to ensure the vehicle heat flux and heat loads meet requirements.

F. Parachute Modeling

The entry vehicle descends using a 8.25 m Disk-Gap-Band (DBG) drogue parachute and 16.7 m ringslot main parachute that are modeled as separate, six-degree-of-freedom rigid bodies. The parachute models developed for Mars Science Laboratory [15] are leveraged with updates derived for Dragonfly. The rigid body includes the canopy, the suspension lines, and the riser. Both parachutes are attached to the entry vehicle with triple bridles, modeled as spring damper elastic tension-only elements. Previous flights have shown modeling the parachute down to the riser as a rigid

body connected with tension-only bridle lines provides vehicle dynamics comparable to flight data [16, 17]. The drogue parachute is mortar-deployed at a defined acceleration using a smart trigger intended to release the parachute at a total angle of attack no greater than 15 degrees to prevent deployment failures. The drogue is sized to prevent the entry vehicle dynamics from becoming unstable while not exceeding a total time of descent or the drogue opening loads requirements. The drogue inflation, peak opening load, static aerodynamics, and apparent mass are modeled. The main parachute is sized to satisfy the lander release velocity requirement while still meeting the descent time constraint. Similarly, the inflation, opening loads, static aerodynamics, and apparent mass are modeled for the main parachute.

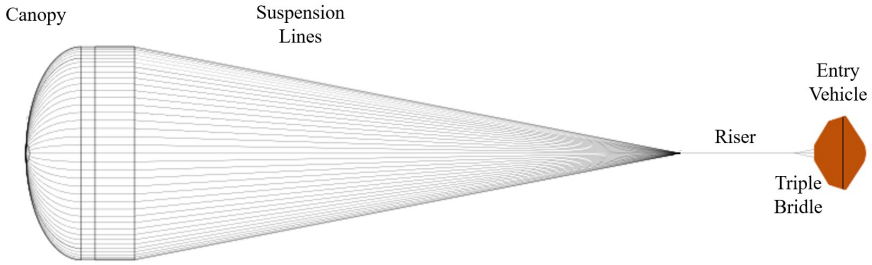

Fig. 7 Main and Drogue Parachute Geometry (not to scale)

G. Aerodynamics

The Dragonfly aerodatabase (ADB) is based on the GSRC ADB [18, 19]. The GSRC free-molecular and hypersonic data was updated using new computational fluid dynamics (CFD) solutions. The subsonic database was modified using data collected from the Langley 12-foot low-speed wind tunnel [20]. Additionally, further improvements were made incorporating data collected from the Langley Transonic Dynamic Tunnel (TDT) [21] and transonic CFD analysis. The ADB provides static aerodynamic axial, normal, and pitching moment coefficients as well as pitch and yaw damping coefficients.

A challenge with leveraging the GSRC OML is the dynamic instability of the vehicle under certain conditions [22], evidenced by the GSRC tumbling when its parachute failed to deploy properly. Fig. 8 shows the statistical distribution pitching damping coefficient, Cmq, of the vehicle from Mach 1.5, prior to drogue deploy, to Mach 0.2. A rule of thumb is that a positive Cmq generally indicates the entry vehicle is dynamically unstable but it is the combination of Cmq and and other factors that determines the stability. References [23] [24] discuss in more depth and show that a small negative Cmq can still be dynamically unstable for the GSRC shape. This has driven design changes to ensure the drogue parachute is robust enough to damp the vehicle's motion and decelerate the vehicle through the most unstable capsule aerodynamic regime.

The ADB changes after the heatshield deploys and characterizes the behavior of the vehicle while the lander is stowed within the backshell or posed for flight. The ADB has been derived using CFD coupled with wind tunnel tests completed at NASA Ames Research Center National Full-scale Aerodynamics Complex (NFAC) tunnel [25, 26]. The model produces forces and moments imparted on the lander and backshell as a function of the velocity, configuration, and the rotor rotation rates. Additionally, the dynamic aero coefficients were derived for both these configurations from data collected at the NASA LaRC Vertical Spin Tunnel [27].

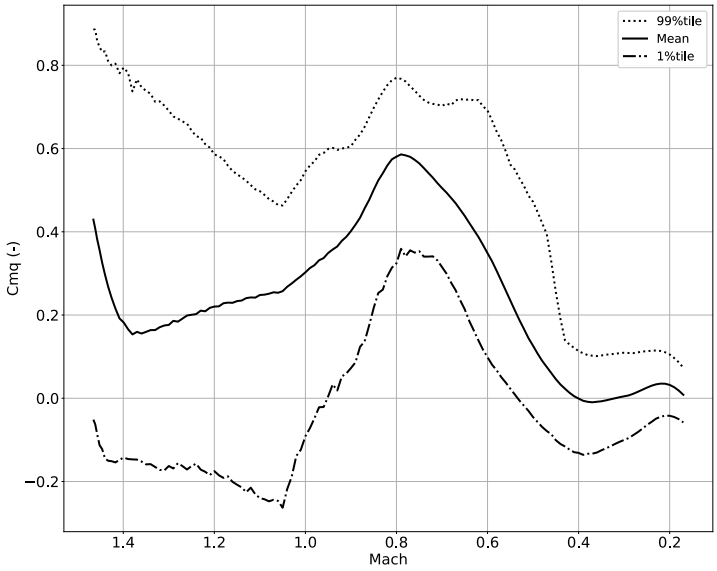

Fig. 8 The pitch damping coefficient of the entry vehicle from Mach 1.5 to 0.2

H. Flight Software and Event Triggers

A flight software (FSW) interface is used in the POST2 simulation to call each FSW model provided by the model developers and interact with vehicle and Titan environment models, and the main POST2 program which contains the dynamics and integration of the simulation as well as input/output, data handling, etc. The flight software interface in POST2 allows for independent control of the data and update rates required from each individual model. The flight software interface also maintains control of spacecraft actuators, inertial measurement unit (IMU), coordinate systems, and landing frame definitions. For the Dragonfly POST2 simulation, the models called through the FSW interface include:

- Drogue Parachute Smart Trigger
- Main Parachute Deployment Trigger
- Pressure Sensors
- Despin Controller
- Lander Separation Logic

Another simulation called the closed loop simulation (CLS) developed by APL is meant to provide more in depth software in the loop (SIL) testing. CLS includes more of the FSW system and autonomy engine as well as detailed hardware models for items such as the rotor motors. CLS is meant to simulate the Dragonfly rotorcraft during free flight and, as such, includes the full guidance, navigation, and control systems. The POST2 simulation will be used to test a smaller set of items such as the IMU, parachute deployment triggers, heatshield separation triggers, and pressure sensors for main parachute deployment.

A number of the separation and configuration change events are activated by timer such as heatshield separation, pose initiation, and the start of despin. The drogue parachute deployment trigger targets a deployment Mach of 1.5 and has a five second window. A sensed acceleration gateway, as measured by the onboard IMU and tuned for each entry opportunity, activates the deployment window. During this window, the drogue deploys via mortar using a smart trigger to minimize the total angle of attack to ensure that the drogue parachute is not deployed into a large cross wind. The end of the five second window is the back up timer if no solution is found by the trigger.

The main parachute is deployed using a pressure sensor to estimate altitude. Since the pressure sensor measurement is a function of the atmosphere, the uncertainty of deployment is large; the pressure sensor model uses a simple Gaussian noise model on top of the truth pressure. The deployment pressure is selected to ensure the heatshield is released at the required altitude and to allow enough timeline for the preparation for powered flight activities.

I. Separation Modeling

POST2 models the cruise stage, heatshield, drogue parachute mortar lid, and lander separation to evaluate near-field and far-field recontact. For near-field recontact, Automated Dynamic Analysis of Mechanical Systems (ADAMS) is used as the primary analysis tool as it has been used for high fidelity multi-body modeling for previous flight projects [28].

The cruise stage separation is modeled using eight separation springs, each with a fault scenario to model off-nominal tip-off behaviors. To track the cruise stage post-separation in POST2, a simplified aerodynamics database was developed for the free-molecular regime and uses modified Newtonian solutions for hypersonics modeling. This is intended to ensure there is no recontact risks with the entry vehicle. Similarly, the heatshield separation is modeled with eight separate spring models. The aerodynamic interaction effects are modeled as suction, as the heatshield separates in the very near distances, and shadowing of the backshell as the heatshield transits through the near- and mid-fields. For the drogue parachute mortar lid separation, the POST2 simulation models it as a 3DOF body and uses a simplified aerodynamics model; the mortar lid is tracked out until about 50 parachute diameters with the separation distance calculated from the lid to both the entry vehicle and the drogue parachute. A simplified lander separation model is included as a secondary check on the primary ADAMS model. The lander is modeled as a separate vehicle in the simulation with its own aerodynamics. The current design calls for guiderails to ensure very near-field separation and this is modeled through a simple translational joint in POST2.

IV. Results

A. Nominal Trajectory

The nominal Dragonfly trajectory is shown in Fig 9 in terms of the planet-relative velocity as a function of altitude with key events highlighted including the Entry Interface (EI), Drogue Parachute Deploy, Main Parachute Deploy, Heatshield (HS) Separation, and the Lander Deploy. Fig. 10 shows the time history of the total angle of attack throughout the descent. It is important to note that after heatshield separation, the vehicle is moving slow enough that descent rates are approximately the same as the zonal wind magnitude. As such, the nadir angle, or the off-vertical angle, is used after HS separation to evaluate the conditions for lander separation as that is the more critical metric for the lander.

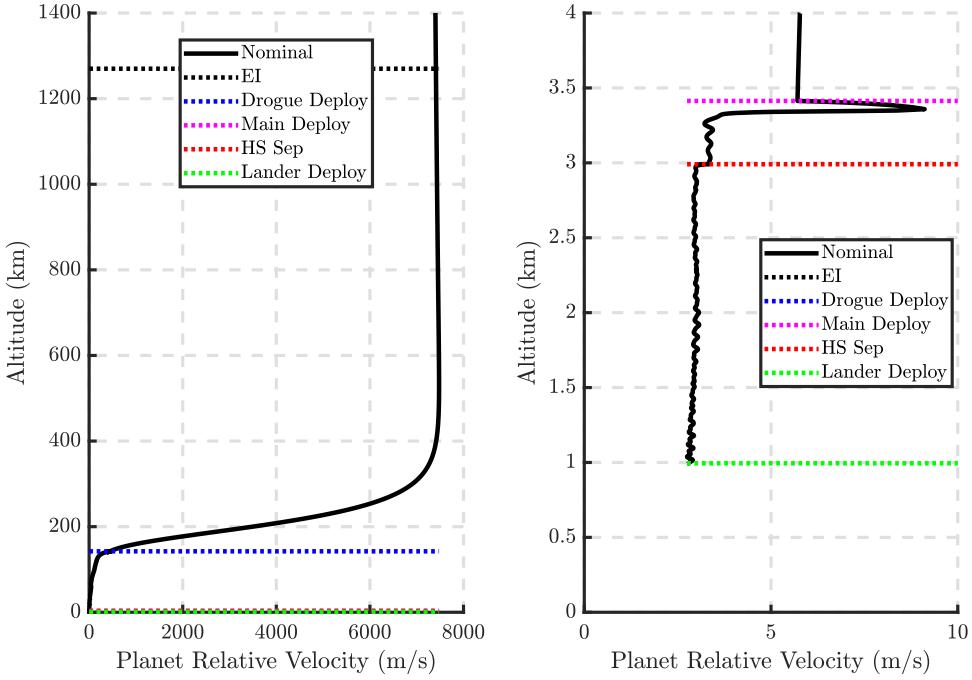

Fig. 9 Nominal altitude vs planet-relative velocity of the entry vehicle

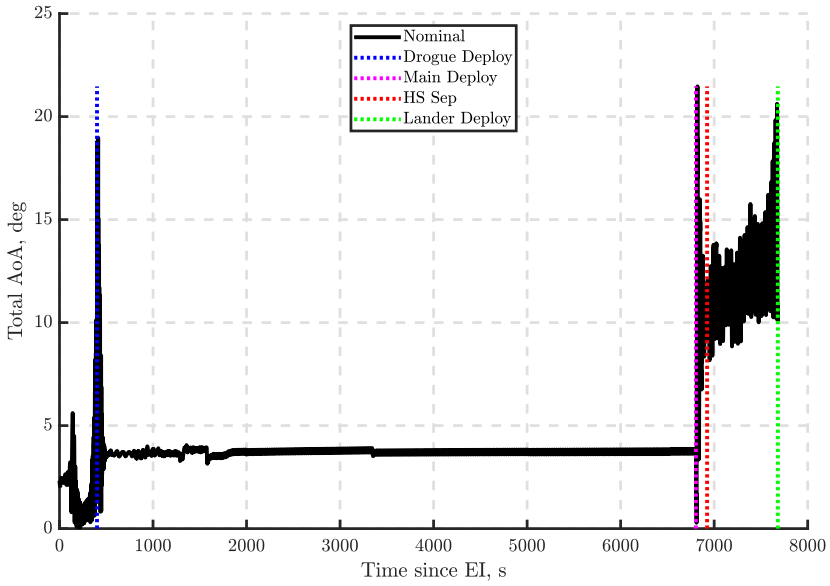

Fig. 10 Total Angle of Attack during EDL

Fig. 11 shows the comparison of the total angle of attack and the nadir angle as the vehicle goes in and out of the winds. Furthermore, Fig. 11 also shows the lateral rate magnitude, which is defined as the root sum square (RSS) of the non-spin attitude rates. Given the current aerodynamics and geometry of the system, the rates are low and stable with minimal impact from the short despin events.

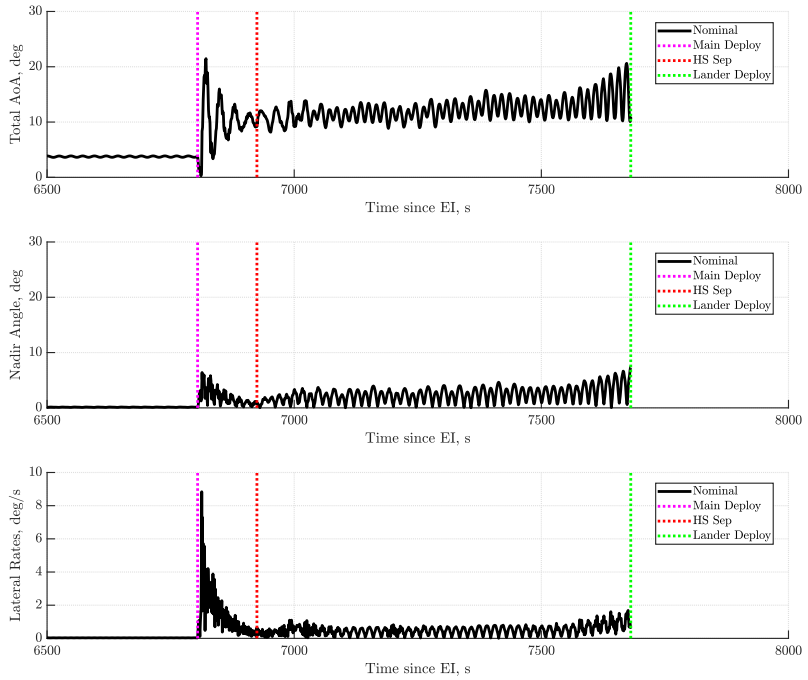

Fig. 11 Total Angle of Attack, Nadir Angle, and Lateral Rates from Main deploy to Lander separation

Another key metric evaluated for the lander deployment is the spin rate of the vehicle during descent shown in Fig.12. Prior to entry, the vehicle is spun up to 2 RPM to provide the entry vehicle stability during entry, with the vehicle later shown to spin up due to the drogue. Currently, there is no skin friction model included for the entry vehicle, but preliminary studies have shown that it would provide a negligible torque. Additionally, the parachute system includes a

swivel to decouple the entry vehicle spin rate from the parachute and no friction is modeled in the swivel. During entry, the vehicle may spin up or spin down depending on the aerodynamic and center of mass uncertainties. The drogue deployment event is a larger driver of the spin rate; large torques are exerted on the entry vehicle and depending on the attitude of both the entry vehicle and the parachute at line stretch and full inflation, the entry vehicle may be spun up or down.

As discussed in section II, after heatshield jettison, the lander's rotors are used to reduce the spin rate of the vehicle to between -4.9 to 4.9 deg/s to ensure lander release conditions and valid images for the optical navigation. The despin controller has two sets of deadbands, an inner deadband to deactivate despin control, -2 to 2 deg/s, and an outer band to activate despin control, -3 to 3 deg/s, which gives the vehicle margin to the requirement and allows the vehicle some robustness in the presence of aerodynamic spin torques in the two seconds prior to lander release. Fig. 13 shows the inner deadband in green and the outer in red; around 7000 seconds is the initial despin event, soon after heatshield separation. In this nominal case, several despin events are illustrated, and there is a one sided spin torque present; the results show the controller consistently activating on the positive spin side of the outer deadband and ending on the other side at the inner deadband as intended. Controller design work is on-going as additional aerodynamic wind tunnel and CFD data is received and incorporated into the aerodatabase.

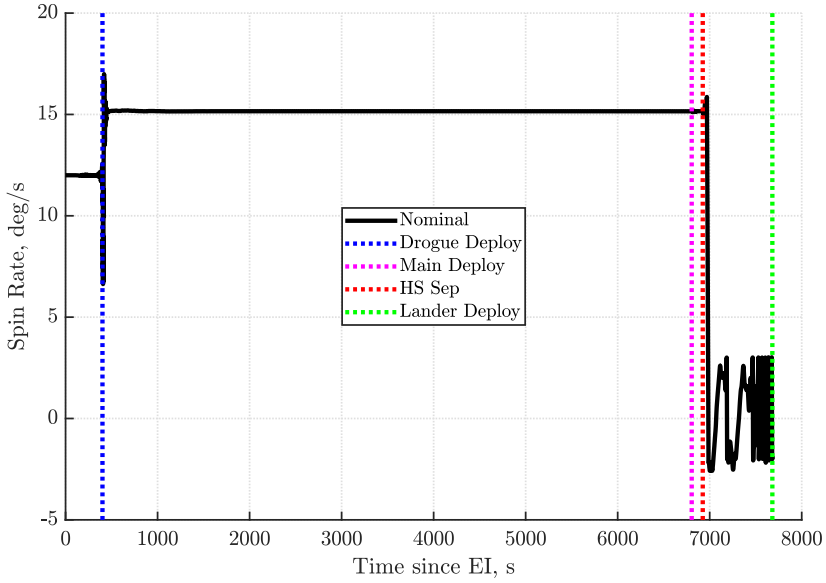

Fig. 12 Spin Rate during EDL

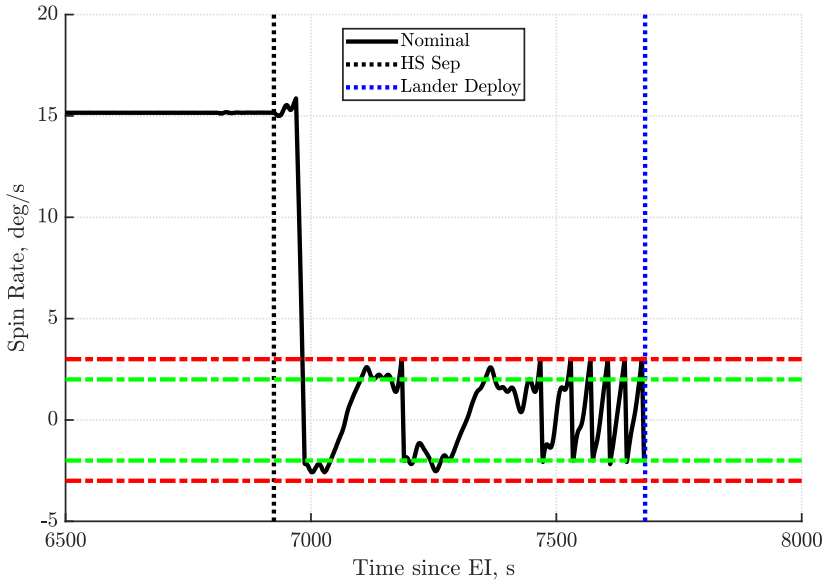

Fig. 13 Spin Rate during from HS Separation to Lander Separation

B. Monte Carlo Results

In order to quantify the robustness of the system, Monte Carlo analysis is conducted using the simulation. A group of input variables are dispersed and statistics on metrics of interest are tracked at specific EDL events. For a typical analysis cycle, the robustness of the design is characterized by analyzing the CBE and MPV mass properties for both launch opportunities using a 10,000 sample Monte Carlo for each scenario. The two launch opportunities are analyzed to ensure the thermal protection system (TPS) design is robust for both scenarios as the entry velocity differs. The two mass property sets are analyzed to ensure the dynamics are understood and characterized for both configurations. For all four baseline scenarios the following uncertainties are modeled in the simulation:

- Initial States & Attitude
- Cruise Stage Separation Spring Stiffness and Spring Failure Modes
- Entry Vehicle Mass Properties
- Cruise Stage Mass Properties
- Atmosphere
- IMU Performance
- Entry Vehicle Aerodynamics
- Drogue Parachute Geometry & Aerodynamics
- Main Parachute Pressure Deploy
- Main Parachute Geometry & Aerodynamics
- Heatshield Separation Spring Stiffness and Spring Failure Mode
- Stowed Vehicle Mass Properties
- Posed Vehicle Mass Properties
- Lander Separation Altitude

These results are used to assess the system's performance against requirements and are provided to the model developers to evaluate their models. Table 1 shows a subset of the performance metrics and the requirements. Table 2 shows the statistical results for all four scenarios.

Table 1 Subset list of performance requirements

Performance Metric	Requirement Type	Value	Units
Peak Entry Load	max	x < 12	g
Max Peak Heat Rate	max	x < 310	W/cm^2
Peak Drogue Opening Load	99%	x < 32	kN
Total AoA @ Drogue Chute Deploy	99%	x < 15	deg
Time to Mach 1.4	99%	x < 10	s
Low Altitude @ Main Deploy	1%	x>=4000	m
High Altitude @ Main Deploy	99%	x<=6000	m
Altitude @ Lander Release	1%	x>800	m
Down Velocity @ Lander Release	99%	x<2.9	m/s
Total Descent Time from Atm interface	99%	x<150	min

Table 2 Subset list of performance metrics assessment for the MPV and CBE mass properties and both launch opportunities

Performance Metric	MPV Primary	MPV Backup	CBE Primary	CBE Backup
Peak Entry Load	100%	100%	100%	100%
Max Peak Heat Rate	100%	100%	100%	100%
Peak Drogue Opening Load	100%	100%	100%	100%
Total AoA @ Drogue Chute Deploy	99.8%	99.5%	99.5%	99.3%
Time to Mach 1.4	100%	99.9%	99.9%	99.4%
Low Altitude @ Main Deploy	99.0%	99.0%	99.1%	99.0%
High Altitude @ Main Deploy	99.8%	99.8%	99.7%	99.6%
Altitude @ Lander Release	100%	100%	100%	100%
Down Velocity @ Lander Release	100%	100%	100%	99.7%
Total Descent Time from Atm interface	100%	100%	100%	99.7%

The number of cases for each Monte Carlo is determined by evaluating how the mean and the 95% confidence interval converge as a function of the number of samples. Fig. 14 shows a subset of the results characterizing how the peak entry loads and the max peak heat rate change as a function of the Monte Carlo sample size. As a result, a baseline Monte Carlo analysis uses 10,000 samples to ensure statistical convergence.

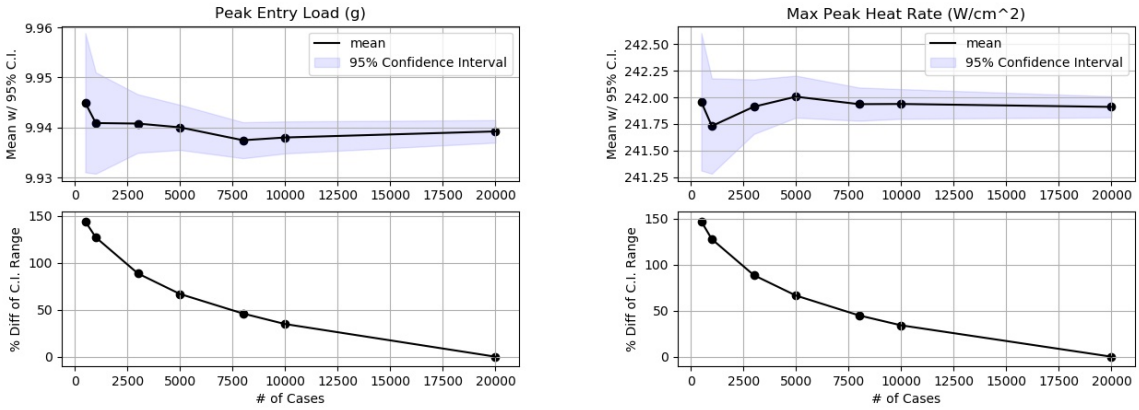

(a) Peak Entry Load

(b) Max Peak Heat Rate

Fig. 14 Statistical Results as a function of Monte Carlo sample size

Furthermore, the Monte Carlo results are evaluated with respect to their requirements and a set of violin plots are generated for each metric to define margins. Fig. 15 - 16 shows the violin plot evaluating the peak entry loads and the max peak heat flux for all four scenarios. In each column, the violin shows the distribution of the Monte Carlo data (note the data is rotated and mirrored). As opposed to a box plot that only shows the ranges of the quartile, the violin plot shows the distribution of the data. The requirement, maximum or 99%-tile, is shown in red. The top of the plot shows the number of standard deviation difference between the 99%-tile or max of the data relative to the requirement. Fig. 15 - 16 shows there is significant margin for peak entry load and heat flux. Fig. 17 shows the spin rate at the pose event before the despin phase; the current metric is to stay within 31 deg/s in either direction. Note the -31 deg/s limit is not shown in in the plot, but the standard deviation to the limit is included in the top. Currently, the vehicle does exceed this metric but the despin aerodynamic torques are large enough to achieve 100% completion to within the desired controller spin rate deadbands.

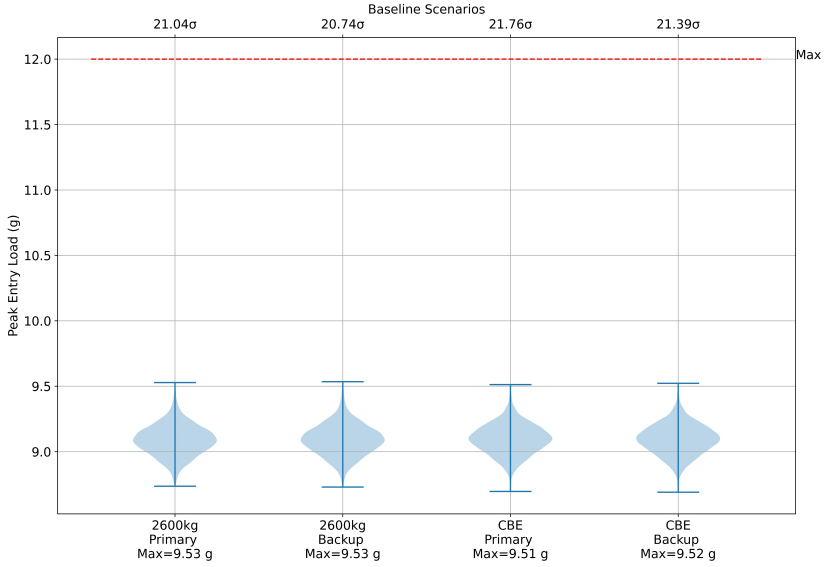

Fig. 15 Violin plots for the peak entry load used to evaluate Monte Carlo results

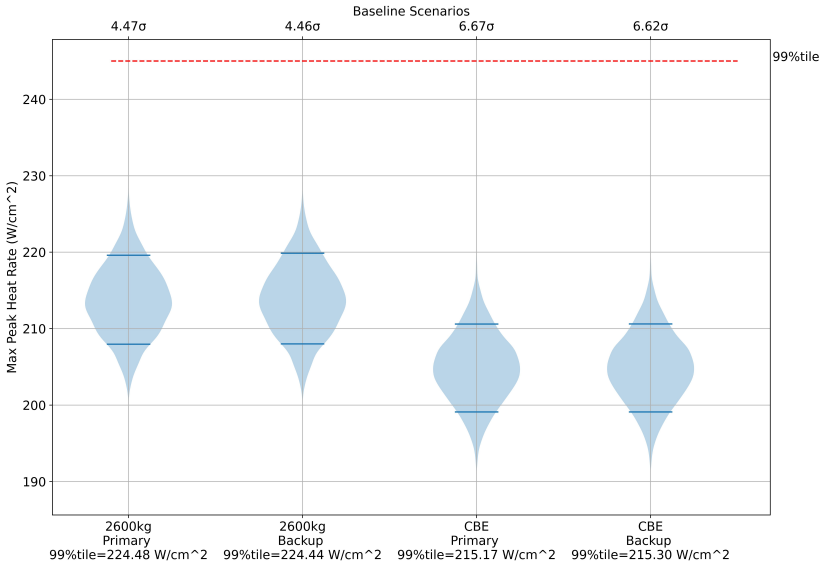

Fig. 16 Violin plots for the peak heat flux used to evaluate Monte Carlo results

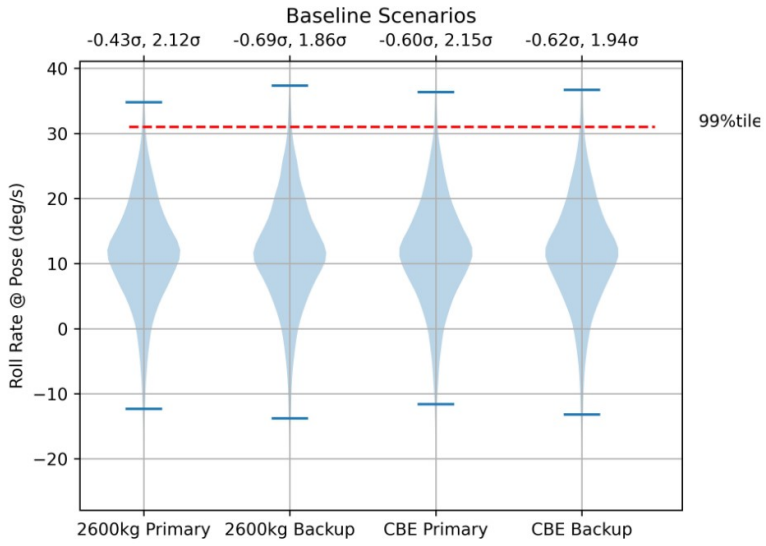

Fig. 17 Violin plot for the spin rate at the pose event

C. Lander Separation Analysis

The lander is set to separate at an altitude of no less than 800 m above the ground within a specified lander separation constraint box or lander release box. Fig. 18 shows the 95% confidence footprint for all four scenarios with respect to the constraint box. The legend characterizes the major and minor axis of the ellipse, the clock angle, and the percent of all trajectories that land within the constraint box. The requirement is defined that 95% of the cases need to be within the box. The percent of trajectories that land within the box is what is assessed with respect to the requirement. The legend shows all cases meet the requirement with the CBE Primary scenario being closest to the requirement. The box is defined by the current understanding of the region where outside of the box is where there is poor radar data, or higher probability of rough terrain. Landing outside the box would not necessarily imply mission failure, therefore the requirement is set as 95% instead of 99%-tile. Fig. 19 - 20 show the sensitivity to the major and minor axes of the footprint with respect to the delivered initial states, mass, atmosphere, entry vehicle aerodynamics, drogue parachute,

and main parachute dispersions as function of time. The atmosphere dispersions, which include temperature, density, winds, and gusts, have the largest contribution for both axes. The zonal winds are the lead contributor to the major axis magnitude by lander separation. Therefore, the end-to-end targeting to the lander release site done by the MDNav and EDL teams is driven by the atmosphere uncertainties.

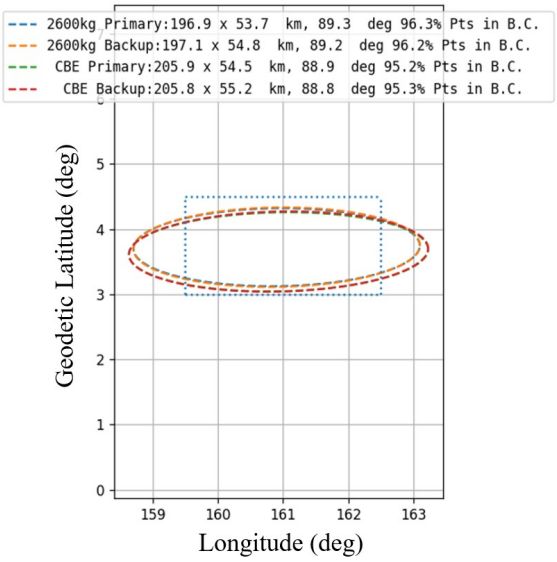

Fig. 18 The Lander separation footprint with respect to the lander separation target box

Fig. 19 The sensitivity of the major axis of the lander separation footprint with respect to the dispersions

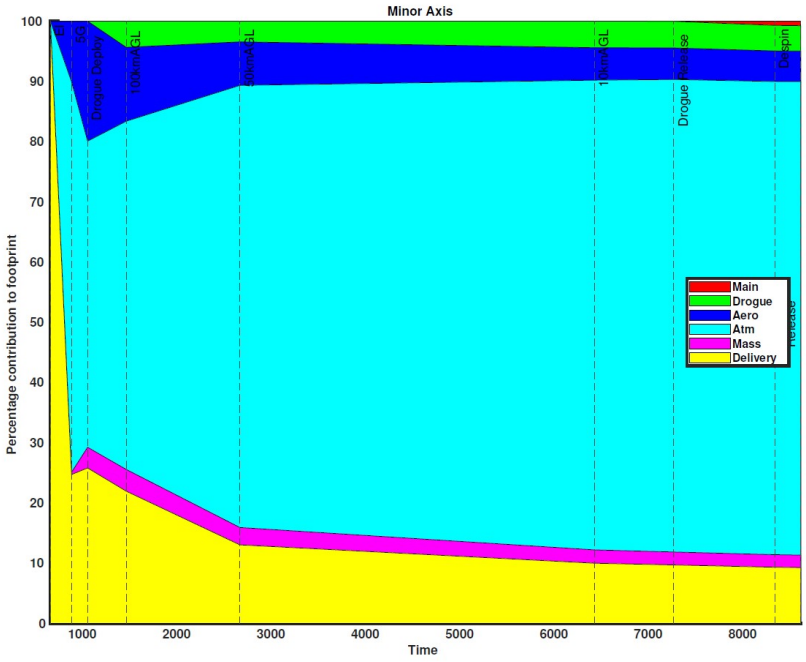

Fig. 20 The sensitivity of the minor axis of the lander separation footprint with respect to the dispersions

V. Conclusion

Dragonfly is a unique mission which will send a rotorcraft to Saturn's moon Titan for the first time in mid 2030s. This mission's novelty presents numerous technical challenges in the design and modeling of Dragonfly. A six-degree-of-freedom flight mechanics simulation has been developed to model the entry and descent trajectory with POST2, evaluating performance metrics to guide design choices. This paper provides a high level overview of models implemented, including updated parachute, aerodynamic, and vehicle mass properties, in POST2 to simulate the EDL dynamics as well as an overview of the Monte Carlo analysis completed. There is ongoing work in supporting model updates, specifically the parachute and aerodynamic models. As the vehicle hardware is manufactured, the mass properties will be further refined and epistemic uncertainties will be reduced. Based on current modeling and simulation, Dragonfly currently meets all of the EDL requirements.

Acknowledgments

The authors would like to thank the Dragonfly team who have been an critical in the development of this simulation.

References

[1] Lorenz, R. D., Turtle, E. P., Barnes, J. W., and Trainer, M. G., "Dragonfly: A Rotorcraft Lander Concept for Scientific Exploration at Titan," *Johns Hopkins APL Technical Digest*, Vol. 34, No. 3, 2018.

[2] Lorenz, R. D., "Dragonfly : Entry and Descent one Titan Year after Huygens," AIAA 2023-0599*, AIAA SciTech 2023,* National Harbor, MD, 2023.

[3] Desai, P. N., and Lyons, D. T., "Entry, Descent, and Landing Operations Analysis for the Genesis Re-Entry Capsule," , Jan. 2005. URL `https://ntrs.nasa.gov/citations/20050060761`, nTRS Author Affiliations: NASA Langley Research Center, Jet Propulsion Lab., California Inst. of Tech. NTRS Meeting Information: 15th AAS/AIAA Space Flight Mechanics Conference; 2005-01-23 to 2005-01-27; undefined NTRS Report/Patent Number: AAS-05-121 NTRS Document ID: 20050060761 NTRS Research Center: Langley Research Center (LaRC).

[4] Winski, R. G., and Pensado, A. R., "Dragonfly Entry and Descent Flight Mechanics Modeling and Analysis," AIAA 2023-0601*, AIAA SciTech 2023,* National Harbor, MD, 2023.

[5] Williams, R. A., Lugo, R. A., Marsh, S. M., Hoffman, J. A., Shidner, J. D., and Aguirre, J. T., "Enabling Thread Safety and Parallelism in the Program to Optimize Simulated Trajectories II," AIAA 2023-0601*, AIAA SciTech 2023,* National Harbor, MD, 2023. https://doi.org/10.2514/6.2023-0148.

[6] Way, D. W., Davis, J. L., and Shidner, J. D., "Assessment of the Mars Science Laboratory Entry, Descent, and Landing Simulation," Kauai, HI, 2013. URL https://ntrs.nasa.gov/citations/20130010129, nTRS Author Affiliations: NASA Langley Research Center, Analytical Mechanics Associates, Inc. NTRS Report/Patent Number: NF1676L-15410 NTRS Document ID: 20130010129 NTRS Research Center: Langley Research Center (LaRC).

[7] Dutta, S., Way, D. W., Zumwalt, C. H., and Blette, D. J., "Postflight Assessment of Mars 2020 Entry, Descent, and Landing Simulation," *Journal of Spacecraft and Rockets*, Vol. 61, No. 3, 2024, pp. 847–857. https://doi.org/10.2514/1.A35771, URL https://arc.aiaa.org/doi/10.2514/1.A35771, publisher: American Institute of Aeronautics and Astronautics.

[8] Shapiro, B. N., Boss, C., Putnam, Z. R., Villac, B., Pensado, A. R., Winski, R. G., and Wright, M., "Dragonfly Preparation for Powered Flight: Lander Separation State Control to Ensure Successful Landing," AIAA 2024-2118*, AIAA SciTech 2024,* Orlando, FL, 2024. https://doi.org/10.2514/6.2024-2118.

[9] Englander, J., Conway, B., and Williams, T., "Automated Interplanetary Trajectory Planning," *AIAA/AAS Astrodynamics Specialist Conference*, 2012. https://doi.org/10.2514/6.2012-4517, URL https://arc.aiaa.org/doi/abs/10.2514/6.2012-4517.

[10] Evans, S., Taber, W., Drain, T., Smith, J., Wu, H.-C., Guevara, M., Sunseri, R., and Evans, J., "MONTE: the next generation of mission design and navigation software," *CEAS Space Journal*, Vol. 10, No. 1, 2018, pp. 79–86. https://doi.org/10.1007/s12567-017-0171-7, URL https://doi.org/10.1007/s12567-017-0171-7.

[11] Mcquaide, M., Ellison, D., Englander, J., Jesick, M., Ozimek, M., and Roth, D., "Dragonfly Phase B Mission Design," , 2023.

[12] Roth, D., "Dragonfly Project: Planetary Constants and Models Document," , 2024. Project Internal.

[13] Naughton, C., Saunders, D., and Brandis, A., "Aerothermal Analysis of the Dragonfly Titan Entry," *21st International Planetary Probe Workshop (IPPW)*, 2024.

[14] Mcbride, B. J., and Gordon, S., "Computer program for calculating and fitting thermodynamic functions," , Nov. 1992. URL https://ntrs.nasa.gov/citations/19930003779, nTRS Author Affiliations: NASA Lewis Research Center, Gordon, Sanford, Cleveland NTRS Report/Patent Number: E-5894 NTRS Document ID: 19930003779 NTRS Research Center: Legacy CDMS (CDMS).

[15] Cruz, J. R., Way, D., Shidner, J., Davis, J. L., Powell, R. W., Kipp, D., Adams, D. S., Sengupta, A., Witkowski, A., and Kandis, M., "Parachute Models Used in the Mars Science Laboratory Entry, Descent, and Landing Simulation," *AIAA Aerodynamic Decelerator Systems (ADS) Conference*, American Institute of Aeronautics and Astronautics, Daytona Beach, Florida, 2013. https://doi.org/10.2514/6.2013-1276, URL https://arc.aiaa.org/doi/10.2514/6.2013-1276.

[16] Cruz, J. R., Way, D. W., Shidner, J. D., Davis, J. L., Adams, D. S., and Kipp, D. M., "Reconstruction of the Mars Science Laboratory Parachute Performance," *Journal of Spacecraft and Rockets*, Vol. 51, No. 4, 2014, pp. 1185–1196. https://doi.org/10.2514/1.A32816, URL https://doi.org/10.2514/1.A32816, publisher: American Institute of Aeronautics and Astronautics _eprint: https://doi.org/10.2514/1.A32816.

[17] Dutta, S., Karlgaard, C. D., Tynis, J. A., O'Farrell, C., Sonneveldt, B. S., Queen, E. M., Bowes, A. L., Leylek, E. A., and Ivanov, M. C., "Advanced Supersonic Parachute Inflation Research Experiment Preflight Trajectory Modeling and Postflight Reconstruction," *Journal of Spacecraft and Rockets*, Vol. 57, No. 6, 2020, pp. 1387–1407. https://doi.org/10.2514/1.A34706, URL https://arc.aiaa.org/doi/10.2514/1.A34706, publisher: American Institute of Aeronautics and Astronautics.

[18] Cheatwood, F., Winchenbach, G., Hathaway, W., and Chapman, G., "Dynamic stability testing of the Genesis Sample Return Capsule," *38th Aerospace Sciences Meeting and Exhibit*, 2000. https://doi.org/10.2514/6.2000-1009, URL https://arc.aiaa.org/doi/abs/10.2514/6.2000-1009.

[19] Desai, P. N., and Cheatwood, F. M., "Entry Dispersion Analysis for the Genesis Sample Return Capsule," *Journal of Spacecraft and Rockets*, Vol. 38, No. 3, 2001, pp. 345–350. https://doi.org/10.2514/2.3707, URL https://doi.org/10.2514/2.3707.

[20] Langley, N., "12 Foot Low-Speed Tunnel (12 FT LST)," https://researchdirectorate.larc.nasa.gov/12-foot-low-speed-tunnel-12-ft-lst/, 2018. Accessed: 2024-10-26.

[21] Langley, N., "Transonic Dynamics Tunnel (TDT)," https://researchdirectorate.larc.nasa.gov/transonic-dynamics-tunnel-tdt/, 2018. Accessed: 2024-10-26.

[22] Desai, P. N., Qualls, G. D., and Schoenenberger, M., "Reconstruction of the Genesis Entry," *Journal of Spacecraft and Rockets*, Vol. 45, 2008, pp. 33–38. https://doi.org/10.2514/1.30042, URL https://arc.aiaa.org/doi/10.2514/1.30042.

[23] Winchenbach, G. L., Chapman, G. T., Hathaway, W. H., Ramsey, A., and Berner, C., "Dynamic Stability of Blunt Atmospheric Entry Configurations," *Journal of Spacecraft and Rockets*, Vol. 39, No. 1, 2002, pp. 49–55. https://doi.org/10.2514/2.3781, URL https://doi.org/10.2514/2.3781.

[24] Schoenenberger, M., and Queen, E. M., "Limit cycle analysis applied to the oscillations of decelerating blunt-body entry vehicles," *NATO RTO Symposium AVT-152 on Limit-Cycle Oscillations and Other Amplitude-Limited, Self-Excited Vibrations*, 2008.

[25] Ames, N., "40- by 80-/80- by 120-Foot Wind Tunnels," https://rotorcraft.arc.nasa.gov/Research/Facilities/windtunnels.html, 2024. Accessed: 2024-10-26.

[26] Edquist, K., "Completion of Dragonfly PPF Testing in the NFAC 80x120-Foot Wind Tunnel," Tech. rep., 2024.

[27] Langley, N., "20-Foot Vertical Spin Tunnel," https://www.nasa.gov/directorates/armd/aetc/20-foot-vertical-spin-tunnel/, 2024. Accessed: 2024-10-26.

[28] Peng, C.-Y., Lih, M., and Ortiz, G., "Development of MSL Rover Loads by Integrated ADAMS-GNC Skycrane Simulation," *MSC Software 2013 Users Conference*, 2013.